Neural Network Analysis of Steel Plate Processing

S. B. Singh, H. K. D. H. Bhadeshia, D. J. C. MacKay†, H. Carey‡ and I. Martin‡

University of Cambridge
Department of Materials Science and Metallurgy
Pembroke Street, Cambridge CB2 3QZ, U. K.

† Cavendish Laboratory
Madingley Road, Cambridge CB3 0HE, U.K.

‡British Steel plc
Swinden Technology Centre
Rotherham, S60 3AR, U. K.

ABSTRACT

The process of rolling is very complicated and the number of parameters which determines the final properties can be quite large. It is extremely difficult therefore to develop a physical model for predicting various properties like yield and tensile strengths. In the present work, a neural network technique which can recognise complex relationships was employed to develop a quantitative method for estimating the yield and tensile strengths as a function of steel composition and rolling parameters. The model was tested extensively to confirm that the predictions are reasonable in the context of metallurgical principles and other data published in the literature.

INTRODUCTION

Cast steel is usually processed into usable products by severe plastic deformation, frequently using the rolling process. The purpose of this deformation is to refine the cast microstructure, to produce the steel in the required shape and to achieve the optimum mechanical properties. The properties depend not only on the deformation but also on the detailed chemical composition in two respects. Firstly, the steel may contain microalloying elements which help control the austenite grain structure and in some cases provide precipitation strengthening [1]. The other alloying additions such as manganese control the relative stabilities of the austenite and ferrite phases and hence the nature of the austenite transformation products.

When a hot ingot or slab enters a rolling mill, its typical dimensions are so large that it has to be reduced to the required thickness in many separate passes. The purpose of the present work was to develop a model enabling the estimation of strength as a function of a large number of rolling parameters and the chemical composition of the steel. The model is based on the neural network analysis technique with a total of 108 variables; the method and the variables are introduced below. The work is restricted to steels with a ferrite and pearlite microstructure.

THE TECHNIQUE

Neural networks are parameterized non–linear models used for empirical regression and classification modelling. Their flexibility makes them able to discover more complex relationships in data than traditional linear statistical models.

A neural network is 'trained' on a set of examples of input and output data. The outcome of this training is a set of coefficients (called weights) and a specification of the functions which in combination with the weights relate the input to the output. The training process involves a search for the optimum non–linear relationship between the inputs and the outputs and is computer intensive. Once the network is trained, the estimation of the outputs for any given inputs is very rapid. The details of the method used here have recently been comprehensively reviewed [2] and the original method is described in references [3–7].

One of the difficulties with blind data modelling is that of 'overfitting', in which spurious details and noise in the training data are overfitted by the model. This gives rise to solutions that generalize poorly. MacKay [3–7] and Neal [8] have developed a Bayesian framework for neural networks in which the appropriate model complexity is inferred from the data.

The Bayesian framework for neural networks has two further advantages. First, the significance of the input variables is quantified automatically. Consequently the model–perceived significance of each input variable can be compared against metallurgical theory. Second, the network's predictions are accompanied by error bars which depend on the specific position in input space. These quantify the model's certainty about its predictions.

THE DATABASE

The neural network method is empirical and hence requires experimental data in order to discover the relationships. The data used were obtained directly from an actual commercial, instrumented plate rolling mill. Given that the work is focused on a production mill, the variables have to be selected from routine records. The input variables therefore consisted of:

(1) The slab reheating temperature, which is universally recognised to be important in determining the initial austenite grain size and the temperature of the slab as it progresses through the rolling mill.
(2) The length of the slab which determines the timing of the rolling process.
(3) The slab gauge; this is of vital importance in determining the total reduction required to achieve the final plate thickness.
(4) The chemical composition, consisting of a total of fourteen different elements.
(5) The rolling parameters, including the pass–by–pass screw settings, any delay period between the passes and the time spent for an individual pass.
(6) The "rolling condition" which is set to 0 for as–rolled plates and 1 for control–rolled or normalised–rolled plates; the latter involved rolling with water cooling, with or without a delay period.

A total of 1892 examples were available for analysis. The maximum number of rolling passes is thirty; when the number is less than thirty, the missing passes were set with zero pass–time, zero delay time and with a roll gap setting which gives zero deformation. The purpose of the analysis was to be able to estimate the yield and ultimate tensile strengths as a function of each one of the 108 variables. Some further information about the variables is given in Appendix 1; that information is necessary in order to reproduce the present work using the trained network.

THE ANALYSIS

Both the input and output variables were first normalized within the range ±0.5 as follows:

$$x_N = \frac{x - x_{min}}{x_{max} - x_{min}} - 0.5 \tag{1}$$

where x_N is the normalized value of x which has maximum and minimum values given by x_{max} and x_{min} respectively.
Linear functions of the inputs x_j are operated on by a hyperbolic tangent transfer function:

$$h_i = \tanh\left(\sum_j w_{ij}^{(1)} x_j + \theta_i^{(1)}\right) \qquad (2)$$

so that each input contributes to every hidden unit (Fig. 1). The bias is designated θ_i and is analogous to the constant that appears in linear regression. The strength of the transfer function is in each case determined by the weight w_{ij}. The transfer to the output y is linear:

$$y = \sum_i w_{ij}^{(2)} h_i + \theta^{(2)} \qquad (3)$$

The specification of the network structure, together with the set of weights is a complete description of the formula relating the inputs to the output. The weights are determined by training the network; the details are described elsewhere [3–7]. The training involves a minimisation of the regularised sum of squared errors. The term σ_ν used below is the framework estimate of the noise level of the data.

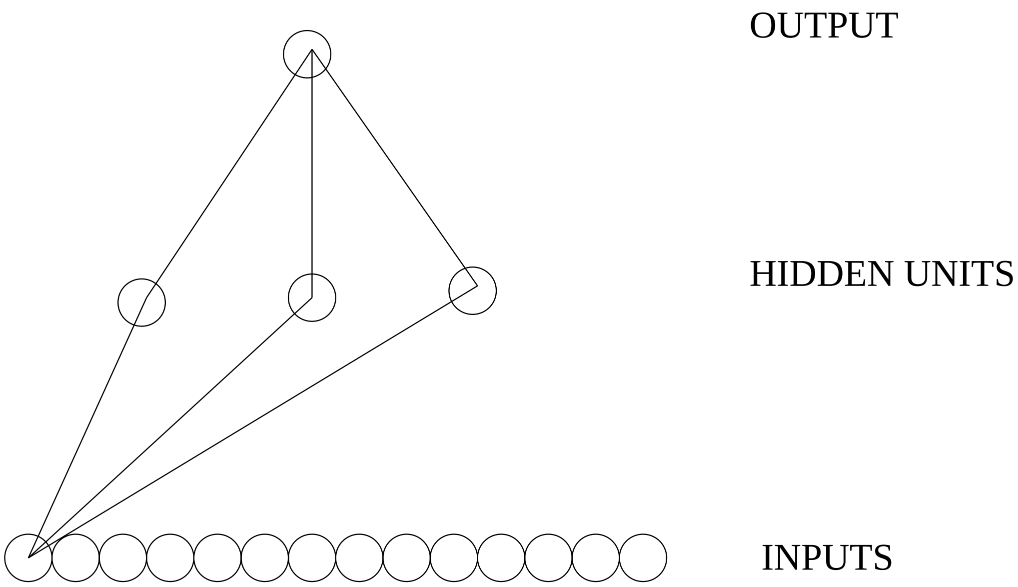

Fig. 1: A typical network used in the analysis. Only the connections originating from one input unit are illustrated, and the two bias units are not illustrated.

NETWORK TRAINING

Yield Strength

The network model for the yield strength consisted of 108 input nodes, a number of hidden nodes and an output node representing the yield strength. The network was trained using 946 of the examples randomly chosen from a total of 1892 available, the remaining 946 examples being kept aside at first to be used as 'new' experiments to test the behaviour of the trained network.

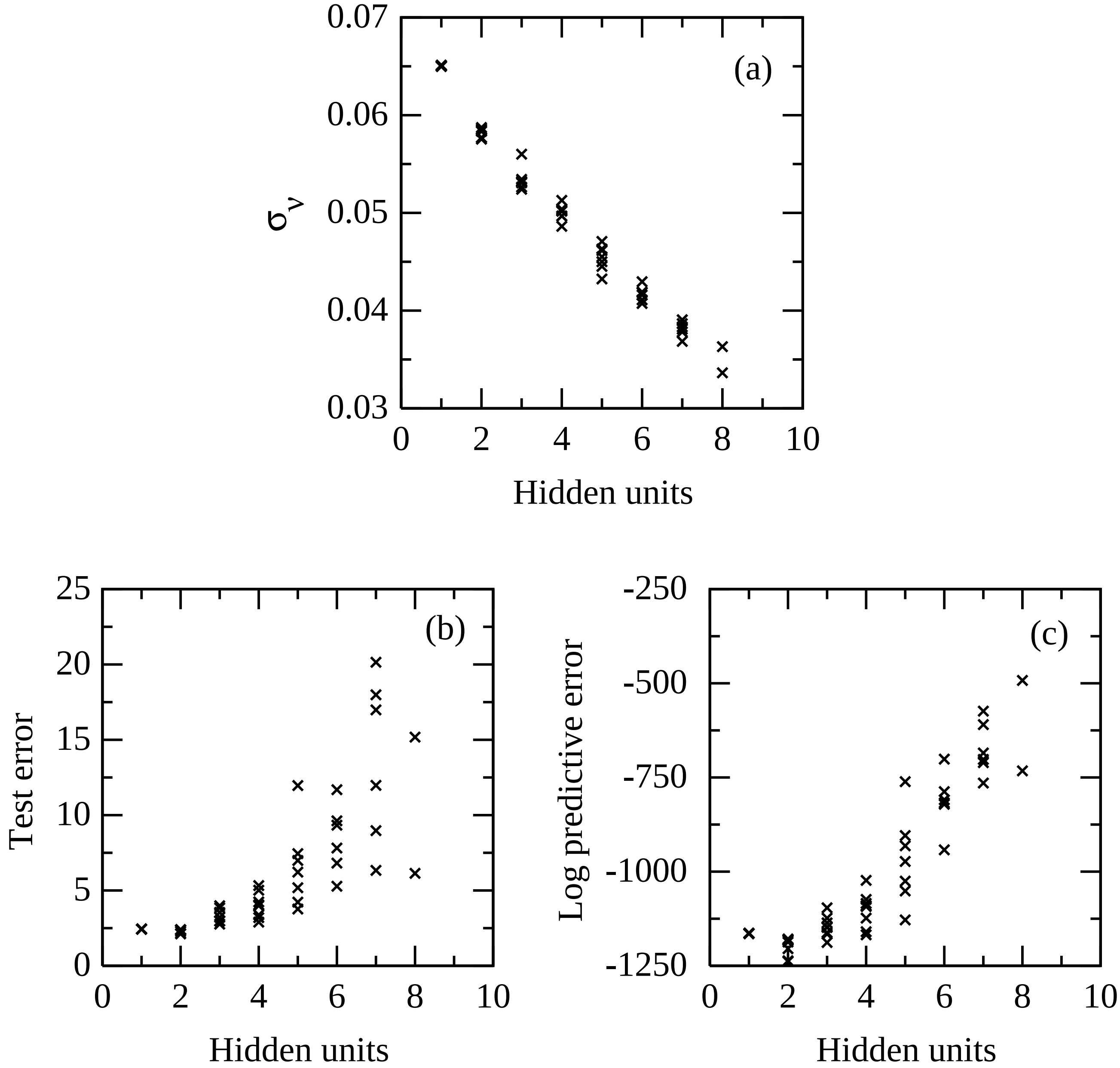

Fig. 2: The YS model: (a) Variation in σ_ν as a function of the number of hidden units, (b) The test error for each of the models, and (c) The log predictive error. Several values are presented for each set of hidden units because the training for each network was started with a variety of random seeds.

The complexity of the model is controlled by the number of hidden units (Fig. 2), and the values of the 110 regularisation constants (σ_w), one associated with each of the 108 inputs, one for biases and one for all weights connected to the output.

Fig. 2a shows that the inferred noise level decreases as the number of hidden units increases. However, the complexity of the model also increases with the number of hidden units. A high degree of complexity may not be justified, and in an extreme case, the model may in a meaningless way attempt to fit the noise in the experimental data. The number of hidden units was set by examining the performance of the model on the unseen test data (Fig. 2b).

A combination of Bayesian and pragmatic statistical techniques were therefore used to control the model complexity. Test error (T_e) is a measure of the deviation of the predicted value from the experimental one in the test data:

$$T_e = 0.5 \sum_n (y_n - t_n)^2 \tag{4}$$

where y_n is the predicted yield strength and t_n is its measured value.

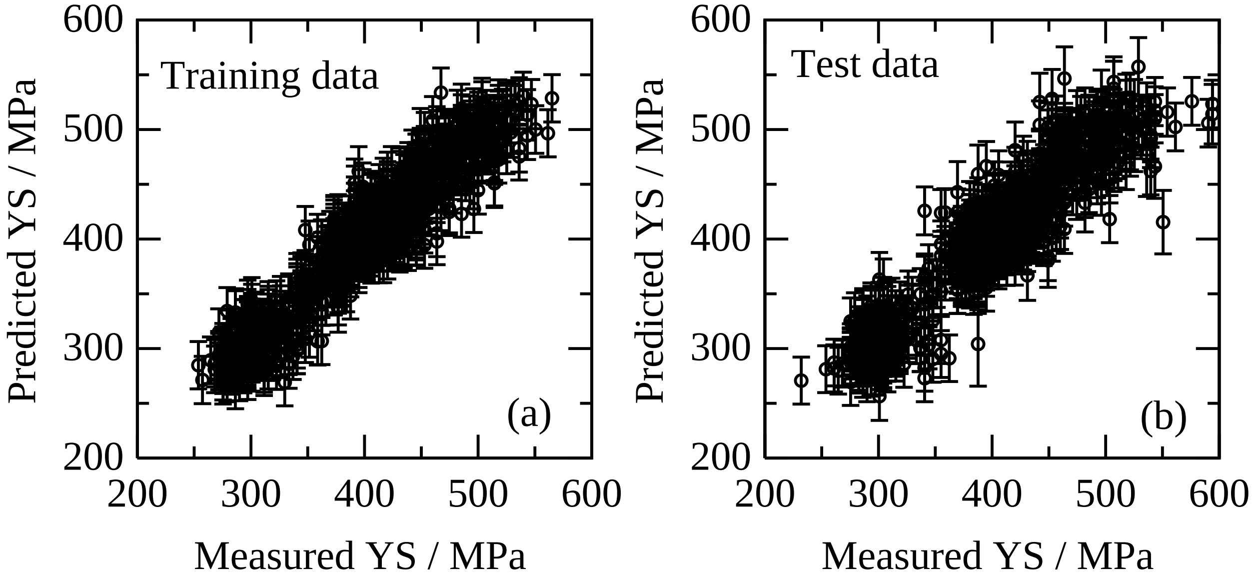

Fig. 3: A comparison between the predicted and measured yield strengths (YS) for the training and test data. The error bars are set to $\pm 1\sigma$ limits and have two components: error bar on the underlying function and the inferred noise level in the data for this model (σ_ν).

It is seen that a model with just two hidden units gives an adequate representation of the data with a minimum in the test error (Fig. 2b). The behaviour of the training and test data is illustrated in Fig. 3 which shows a similar degree of scatter in both the graphs, indicating that the complexity of this particular model is optimum. It should be noted that the test data cover a wider range of yield strength values and for a few cases at the highest yield strengths, the model underpredicts the measured values. Over–fitting would lead to an apparently better accuracy in the prediction of training data when compared with the test dataset. The error bars in Fig. 3 include the error bars on the underlying function and the inferred noise level in the dataset (σ_ν). In all other subsequent predictions discussed below the error bars include the former component only. The test error is one measure of the performance of a model. Another useful measure is the "log predictive error" [3–6] for which the penalty for making a wild prediction is much less if the wild prediction is accompanied by an appropriately large error bar. Assuming that for each example n the model gives a prediction with error, (y_n, σ_n^2), the log predictive error (LPE) is:

$$LPE = \sum_m \left[\frac{1}{2} \left(t_n - y_n \right)^2 / \sigma_n^2 + \log(\sqrt{2\pi}\sigma_n) \right] \tag{5}$$

When making predictions, Mackay [5] has recommended the use of multiple good models instead of just one best model. This is called 'forming a committee'. The committee prediction, $\overline{y}$, is obtained using the expression:

$$\overline{y} = \frac{1}{L}\sum_{i} y_i \tag{6}$$

where L is the size of the committee and y_i is the estimate of a particular model i. The optimum size of the committee is determined from the validation error of the committee's predictions using the test dataset. The test error of the predictions made by a committee is calculated by replacing the y_n in equation (4) with $\overline{y}$. In the present analysis a committee of models was used to make more reliable predictions. The models were ranked according to their log predictive error. Committees were then formed by combining the predictions of best M models, where M gives the number of members in a given committee model. The test errors for the first 18 committees are shown in Fig. 4.

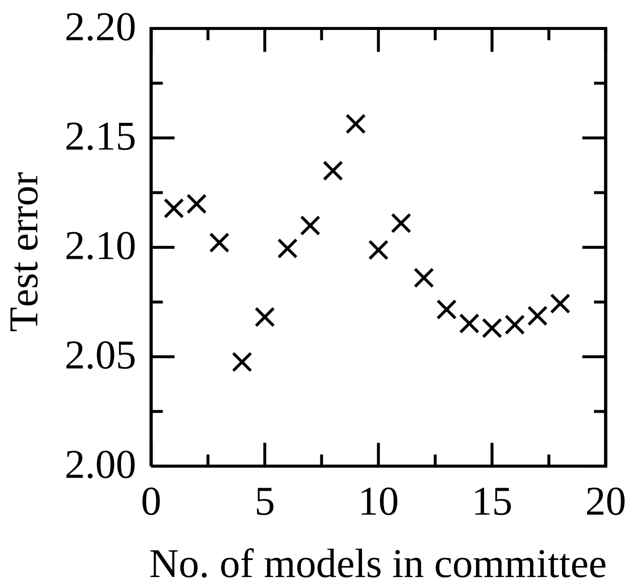

Fig. 4 : The test error as a function of the number of members in a committee of YS models.

A committee of the best four models gives the minimum error; three of these were two hidden unit models and the remaining one was a three hidden unit model. Each constituent model of the committee was therefore retrained on the entire dataset beginning with the weights previously determined. Fig. 5 shows the results from the new training on the entire dataset. For the sake of simplicity, the error bars in Fig. 5 include the error on the fitted function only.

The Ultimate Tensile Strength

The same procedure was used to model the ultimate tensile strength (UTS), with the same set of 108 input variables. The variation in σ_ν, the test error and log predictive error with the number of hidden units is shown in Fig. 6.

The model with two hidden units was found to be the optimum one and a committee of the nine best models led to a further reduction in the test error, as illustrated in Fig. 7.

The results of the retraining of the committee model on the all of the data are illustrated in Fig. 8.

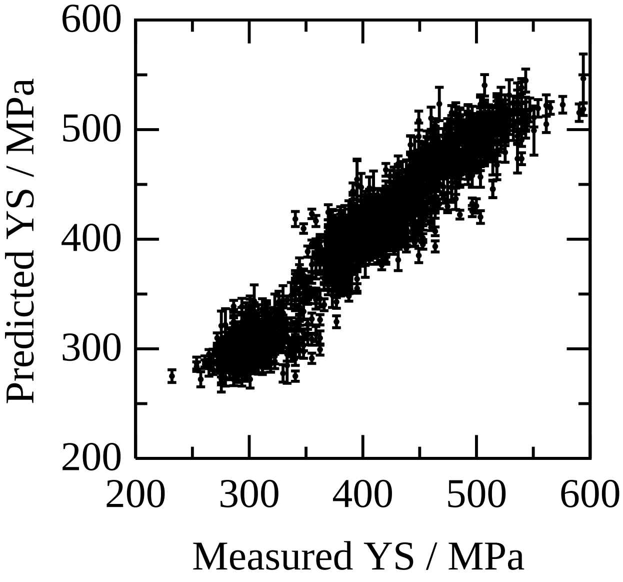

Fig. 5: Training data for the best yield strength commitee model, training was done on the whole dataset. The error bars include the error in the underlying function only.

APPLICATION OF THE MODELS

The optimised committee models were used to study the effect of individual variables on the yield strength and the tensile strength in order to see whether the results are compatible with known metallurgical principles and other published data. These studies are limited to simple relationships since there are no metallurgical models which deal with all the variables incorporated in the neural network approach.

In the discussion that follows, a typical 19 pass schedule with a starting slab thickness of 200 mm and the final pass screw setting of 13.8 mm was used unless otherwise stated. The slab reheating temperature was set at 1215 °C. The chemical compositions were set at their average concentrations listed in Appendix 1. A comprehensive list of the standard set of variables is presented in Table 1 in the precise order in which they appear in Appendix 1. For example, a variation in the carbon concentration is discussed leaving all the other variables in Table 1 unchanged. In all the predictions below, the error bars represent the $\pm 1\sigma$ limits on the underlying function.

Carbon Concentration

It is well known that carbon forms an interstitial solid solution in iron, leading to intense solid solution strengthening. The effect is more pronounced in the case of ferritic iron because unlike austenite, the carbon atoms cause a tetragonal distortion of the lattice giving strong interactions with all kinds of dislocations [9]. It has been estimated that 1 wt.% C in solid solution in ferrite raises the yield strength by 4600 MPa and UTS by 6800 MPa [10]. However, the solubility of carbon in ferrite is extremely small so that the main effect in the context of steels with a mixed microstructure of ferrite and pearlite is to increase the fraction of the latter phase. There is also a refinement of microstructure since the temperature at which the ferrite forms is suppressed. Both the yield and tensile strengths should therefore increase with the carbon concentration and this is indeed replicated by the model (Fig. 9); the calculations are for a steel without Nb or V additions. Note also that as must be expected, the UTS is always predicted to be higher than the yield strength even though the latter was not included as an

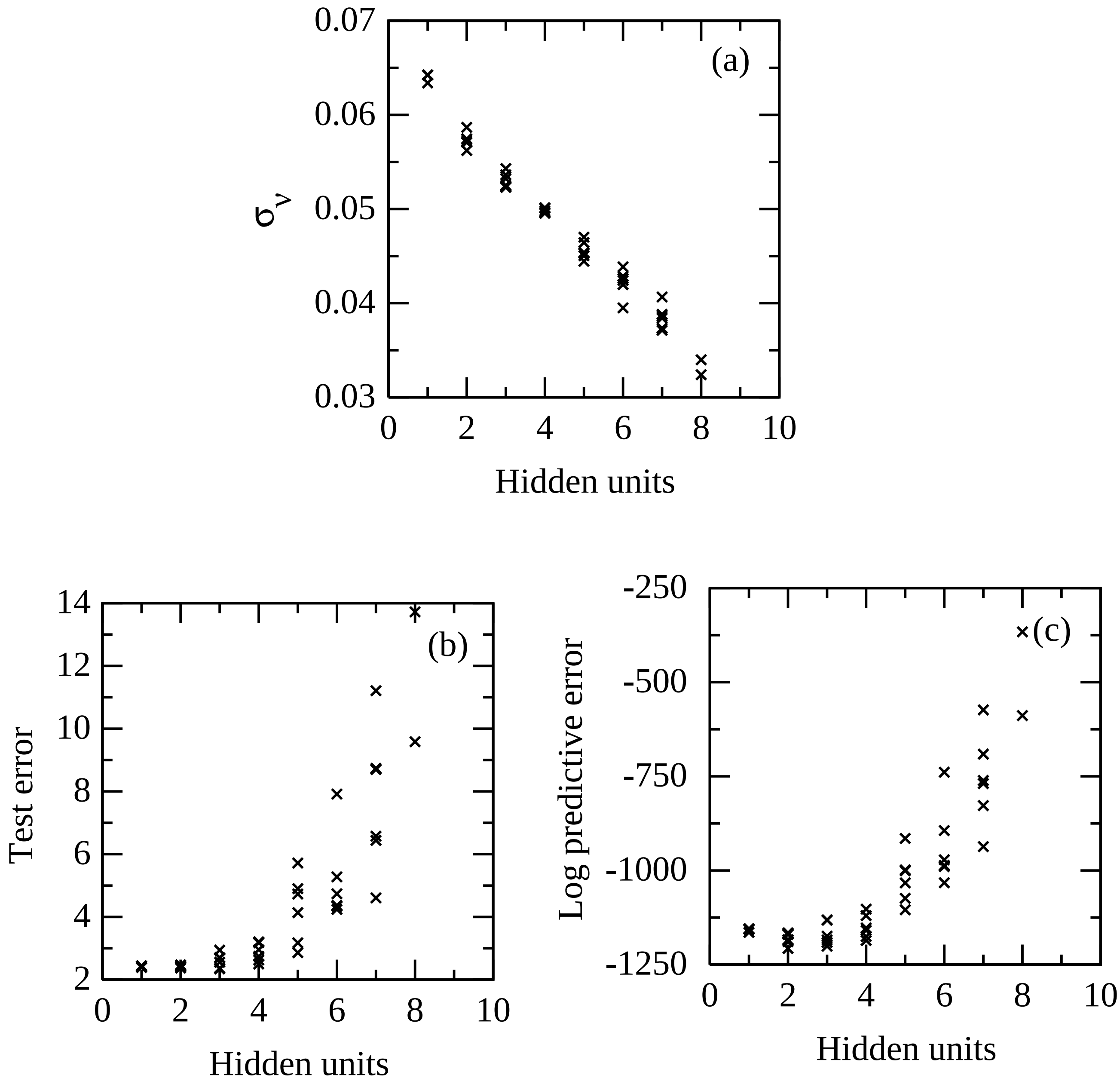

Fig. 6: The σ_ν and errors as a function of the number of hidden units for the UTS models. Several values are presented for each set of hidden units because the training for each network was started with a variety of random seeds.

input to the UTS model. The error bars ($\pm 1\sigma$) are larger when an attempt is made to predict at concentrations beyond the range of the training dataset. The yield strength increases by about 32 MPa (ignoring the error bars) when the concentration is increased from 0.025 to 0.25 wt.%. This is consistent with experimental data by Hodgson and Gibbs [11] who found an increase in the lower yield strength by about 15 MPa for a 0.1 wt.% increase in the carbon concentration.

Consistent with experimental observations [10,12,13] the UTS is predicted to be more sensitive to the carbon concentration than the yield strength (Fig. 9). The predominant effect of carbon in the steels considered here is to increase the pearlite fraction in the microstructure. For carbon concentrations up to 0.3 wt.% where the pearlite fraction is relatively small, yielding

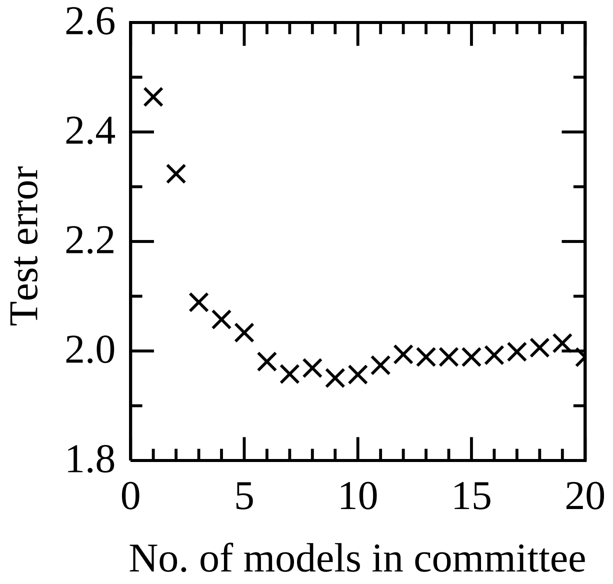

Fig. 7: The test error as a function of the number of members in a committee of models for UTS.

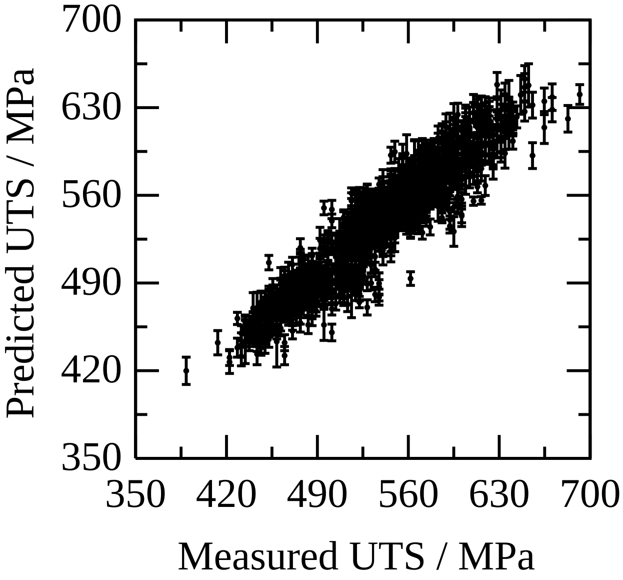

Fig. 8: Training data for the best UTS commitee model, training was done on the whole dataset.

begins in the softer ferrite which has to work harden before the pearlite starts to undergo plastic deformation. As a consequence, the effect of pearlite on the yield strength is smaller. On the other hand, pearlite content does affect the UTS because it is associated with large plastic strains where all phases must participate in deformation. These observations are also reflected in Pickering's [10] regression equations for similar steels, where the quantity of pearlite freatures only in the UTS equation:

$$\text{YS, MPa} = 53.9 + 32.3w_{Mn} + 83.2w_{Si} + 354.2\sqrt{w_{N\mathrm{f}}} + 17.4(d^{-0.5}) \tag{7}$$

$$\text{UTS, MPa} = 294.1 + 27.7w_{Mn} + 83.2w_{Si} + 3.85(\%\text{pearlite}) + 7.7(d^{-0.5}) \tag{8}$$

where w represents the concentration of the element identified by the subscript, in weight percent, N_f is the free nitrogen, d is the ferrite grain size in mm.

1215.0	200.0	2760.0	0.140	1.260	0.320	0.007	0.015	0.031
0.030	0.003	0.025	0.037	0.005	0.023	0.009	0.002	174.0
158.0	2.0	149.6	8.0	4.0	141.3	23.0	1.0	133.6
7.0	1.0	125.9	6.0	2.0	118.3	5.0	2.0	110.0
6.0	2.0	105.1	16.0	3.0	85.1	24.0	3.0	70.7
7.0	3.0	58.6	6.0	3.0	48.7	7.0	3.0	40.1
7.0	4.0	33.0	6.0	5.0	22.9	36.0	6.0	15.8
7.0	9.0	14.9	6.0	9.0	14.1	7.0	10.0	13.8
7.0	10.0	13.8	0.0	0.0	13.8	0.0	0.0	13.8
0.0	0.0	13.8	0.0	0.0	13.8	0.0	0.0	13.8
0.0	0.0	13.8	0.0	0.0	13.8	0.0	0.0	13.8
0.0	0.0	13.8	0.0	0.0	13.8	0.0	0.0	7

Table 1: Table of variables used for the predictions. The variables appear in the same sequence as they appear in Appendix 1.

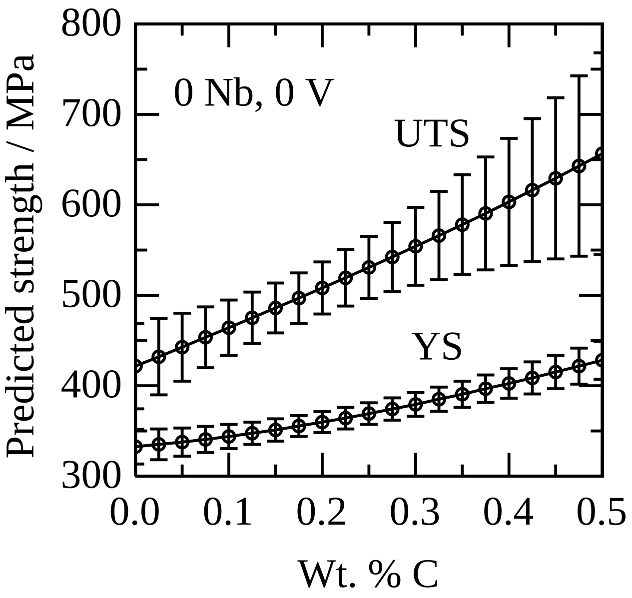

Fig. 9: The variation of yield and ultimate tensile strength with carbon for a steel without any microalloying additions. The error bars represent $\pm 1\sigma$ limits.

Based on a study covering a wide range of ferrite grain sizes in a number of C steels Morrison [14] found a slightly different factor of 18.13 for the effect of ferrite grain size on the yield strength (equation 7).

Fig. 10a shows calculations for a microalloyed steel with 0.03 wt.% Nb. Fig. 10b illustrates on the same scale, the effect of increasing pearlite content on the UTS as calculated using equation 8 (the zero carbon result is from the neural network model). The agreement between the two is excellent and similar results have been reported by Shimizu *et al.* [12]

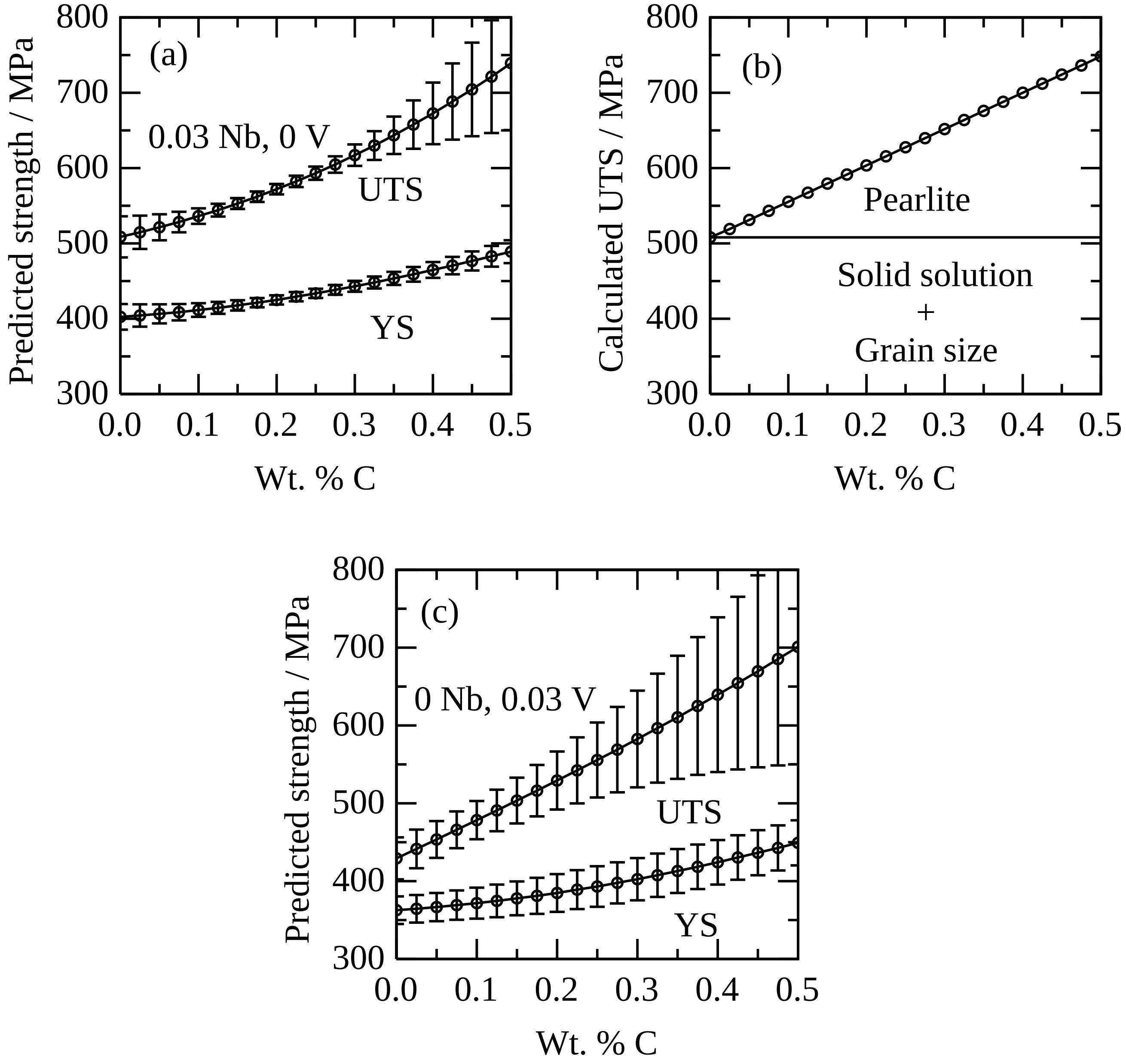

Fig. 10: The effect of (a) carbon; (b) pearlite content on the yield and ultimate tensile strengths of a microalloyed steel containing 0.03 wt.% Nb (zero vanadium). (c) The yield and ultimate tensile strengths for a 0.03 wt.% vanadium microalloyed steel (zero niobium). Other elements were as in Table 1. The UTS in (b) was calculated using equation 8 [10]

.

A comparison of Figs. 9 and 10a shows that the addition of 0.03 wt.% Nb to a plain C–Mn steel raises both the yield and ultimate tensile strengths by about 65 MPa at all carbon concentrations. A corresponding addition of 0.03 wt.% V increases the strength by only about

20 MPa (Fig. 10c). It is well known that niobium is more effective in restricting recrystallisation than vanadium [15, 16]. The reason for this is discussed separately.

The starting slab thickness was set at 200 mm and the final plate thickness 13.8 mm in all of the above calculations. If this is changed to a 400 mm initial thickness but the rolling schedule is kept the same (*i.e.* the same percentage pass reductions and the pass and interpass times) then the final plate thickness becomes 27.7 mm. This should lead to a reduction in the strength because the cooling rate when rolling is completed will be slower for a thicker plate and because the rolling reductions occur at relatively higher temperatures (the thicker slab spends the same time in the mill). The finish rolling temperature will be higher for 27.7 mm plate compared with 13.8 mm plate. The reduction in strength is predicted by the neural network as illustrated in Fig. 11, although there is some uncertainty due to the large error bars for the UTS calculations. It needs to be emphasized that an initial slab thickness of 400 mm is simply used as an example here to test the model predictions. In actual practice, the initial slab thickness is typically in the range of 225–305 mm. Or alternatively, ingot of an initial thickness of 600 mm is used.

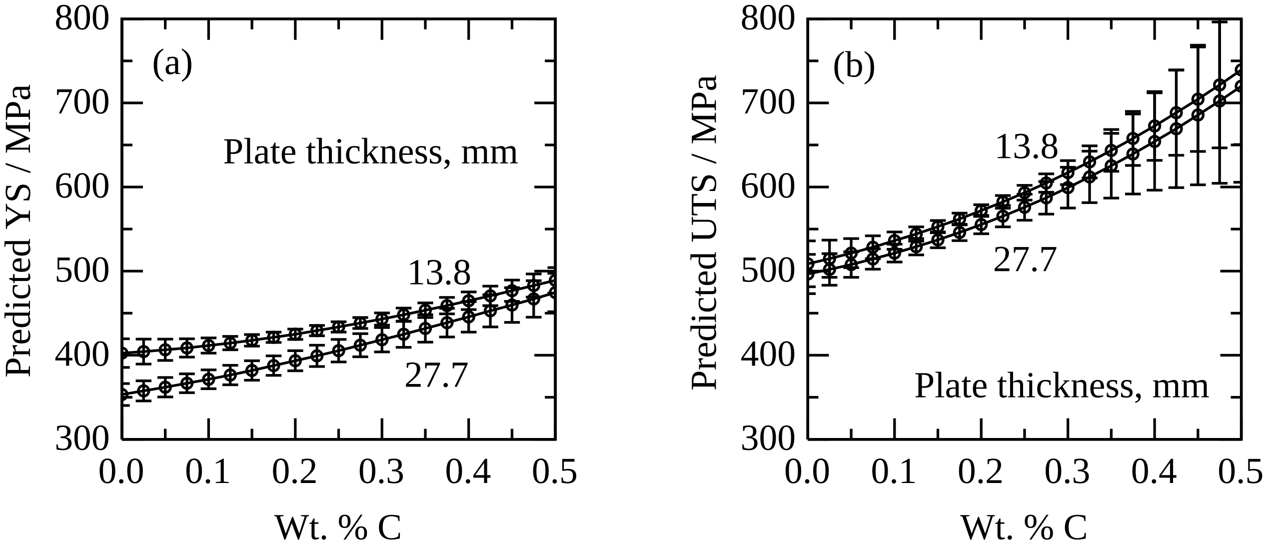

Fig. 11: The effect of plate thickness on the yield and ultimate tensile strengths of a niobium microalloyed steel as a function of the carbon concentration.

Manganese Concentration

Manganese not only provides solid solution strengthening but also has a strong effect on the stability of the austenite. It lowers the ferrite transformation temperature and therefore leads to a refinement of microstructure [17]. Manganese also shifts the eutectoid point to lower carbon concentrations and thus leads to an increase in the volume fraction of pearlite.

The Pickering equations given above [10] attribute a 32 and 27 MPa solid solution strengthening increment in the yield and ultimate tensile strengths respectively due to a 1 wt.% increase in the manganese level. The predictions in Fig. 12a,b include all the effects of manganese and hence the somewhat larger strength increment is consistent with the smaller values reported by Pickering. The results are in agreement with the work of Gladman *et al.* [18] for a normalised steel.

As with carbon, an increase in the plate thickness led to a decrease in strength (Fig. 12c,d). The increase in thickness was achieved by doubling the slab thickness whilst keeping the same rolling schedule. The reduction in the yield strength is larger than in the UTS, presumably because the former is more sensitive to grain size (equations 7 and 8).

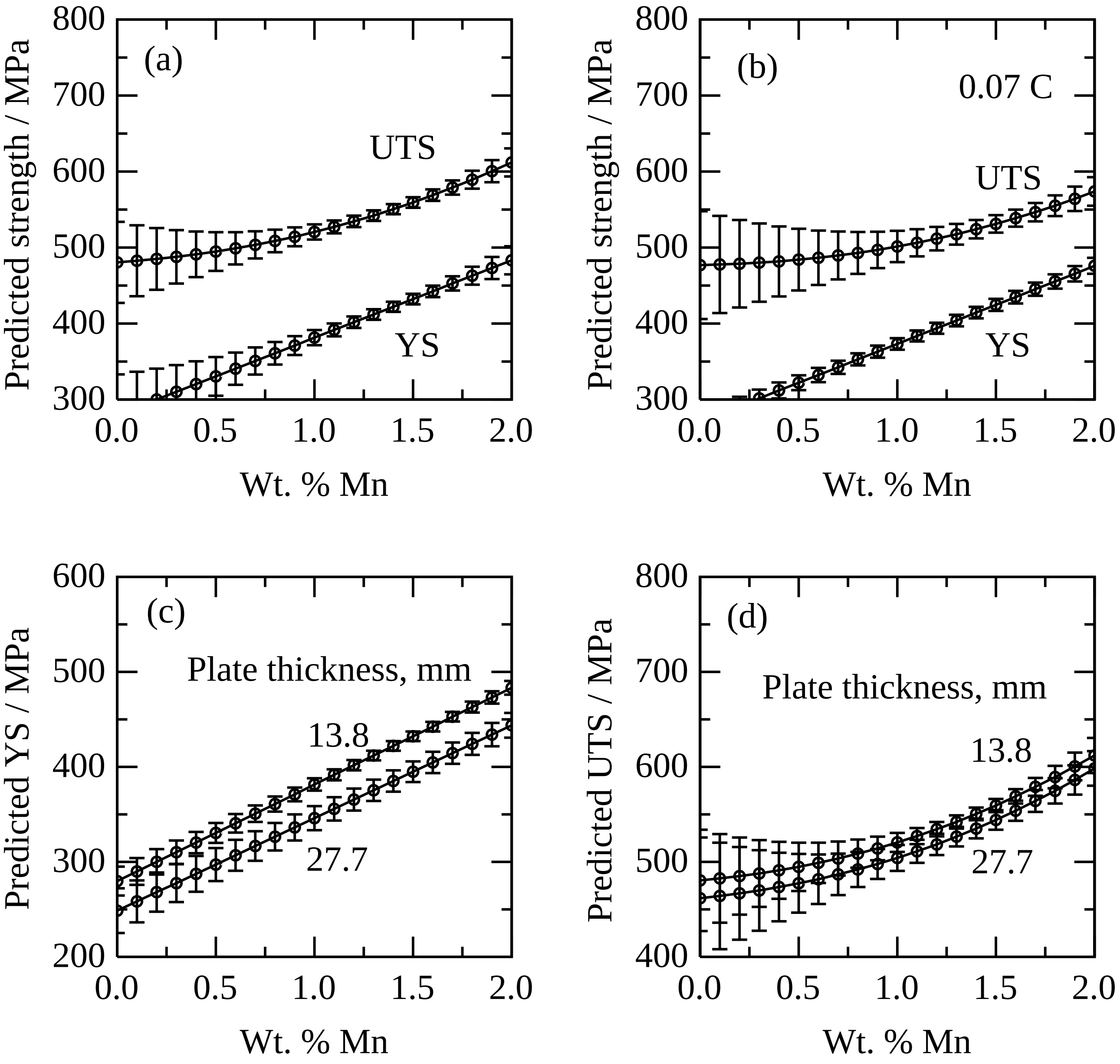

Fig. 12: (a, b) The yield and ultimate tensile strengths as a function of the manganese content. (c, d) The effect of manganese concentration and plate thickness on strength. The thickness was increased by doubling the initial slab thickness.

It is a common practice during thermomechanical processing to hold the slab at an intermediate stage during rolling for a certain length of time. This allows it to cool to a pre–determined temperature before rolling is resumed. The temperature is then sufficiently low to prevent the austenite from recrystallising during deformation. The deformation and the increase in austenite surface area per unit volume due to its pancaked shape enhances the ferrite nucleation rate, giving grain refinement and a corresponding increase in strength. This behaviour is predicted as illustrated in Fig. 13. The delay period before the 9 th pass was increased from 24 to 700 seconds, this would have the effect of lowering both the end hold temperature and the finish rolling temperature with a consequent increase in the yield and the tensile strengths (Fig. 13).

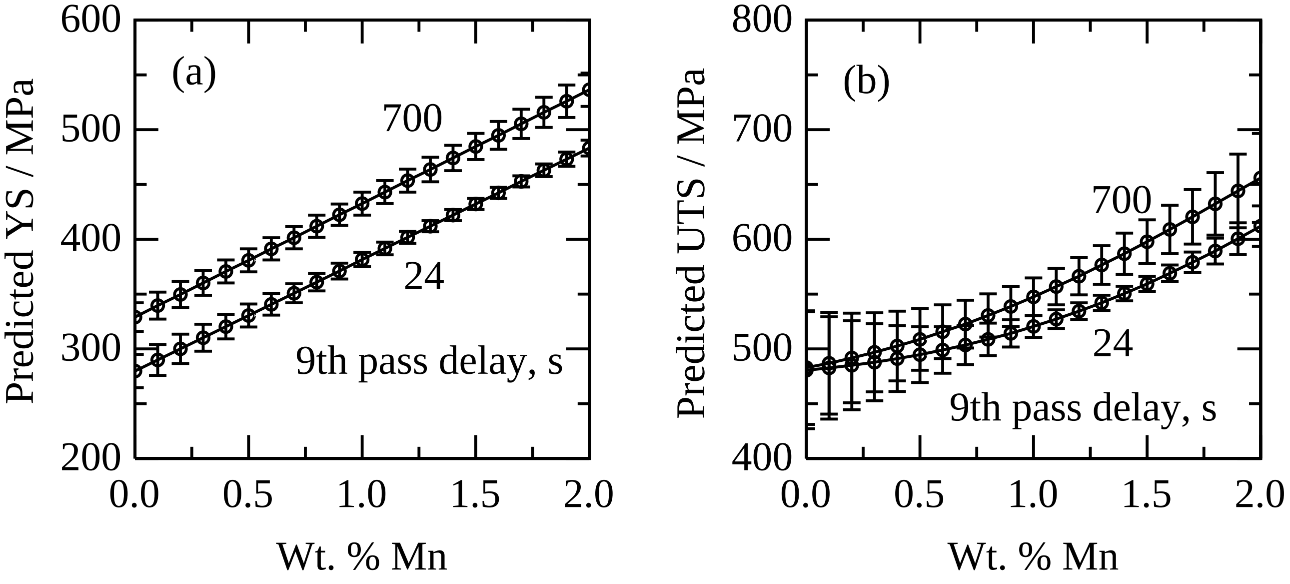

Fig. 13: The effect of a delay period before the 9 th pass on the strength for a range of manganese concentrations.

If the increase in the strength is assumed to be due to grain refinement then according to the Pickering regression equations 7 and 8, the increase in YS should be 1.13/0.5 times the rise in UTS. The model predictions are in excellent agreement with this. For a 1.3 wt.% Mn steel the YS increases by 52 MPa whereas UTS increases by 23 MPa (Fig. 13). Thus, it might be argued that a delay of 700 seconds before the 9 th pass is equivalent to an addition of about 0.025 wt.% of costly Nb. These factors are consistent with the mill experience though in actual practice, it is the concentration of C and/or Mn which is reduced rather than that of Nb to improve the weldability and toughness. However, a hold of as large a period as 700 seconds has other commercial implications. It amounts to a total loss of production; in 700 seconds two plates can be rolled to schedules which do not involve long delay periods.

The calculations carried out for manganese were repeated for silicon in concentrations up to 1 wt.% but it was found not to have any significant effect on the strength. Silicon raises the ferrite transformation temperature and this might compensate for its solid solution strenghening.

Microalloying Additions

Niobium and vanadium carbonitrides prevent austenite grain coarsening during reheating [19]. They also help refine the austenite grain structure during hot–rolling by pinning the grain boundaries and retarding recrystallisation [19]. Nb is the most effective microalloying addition for suppressing the recrystallisation, Fig. 14 [20]. This is also evident from the regression equation proposed by Boratto *et al.* [21]:

$$T_{nr} = 887 + 464w_C + (6445w_{Nb} - 644\sqrt{w_{Nb}}) + (732w_V - 230\sqrt{w_V}) + 890w_{Ti} + 363w_{Al} - 357w_{Si} \tag{9}$$

where T_{nr} is the no recrystallisation temperature *i.e.* the temperature below which recrystallisation is very sluggish and w represents the concentration, in weight percent, of the element identified by the subscript.

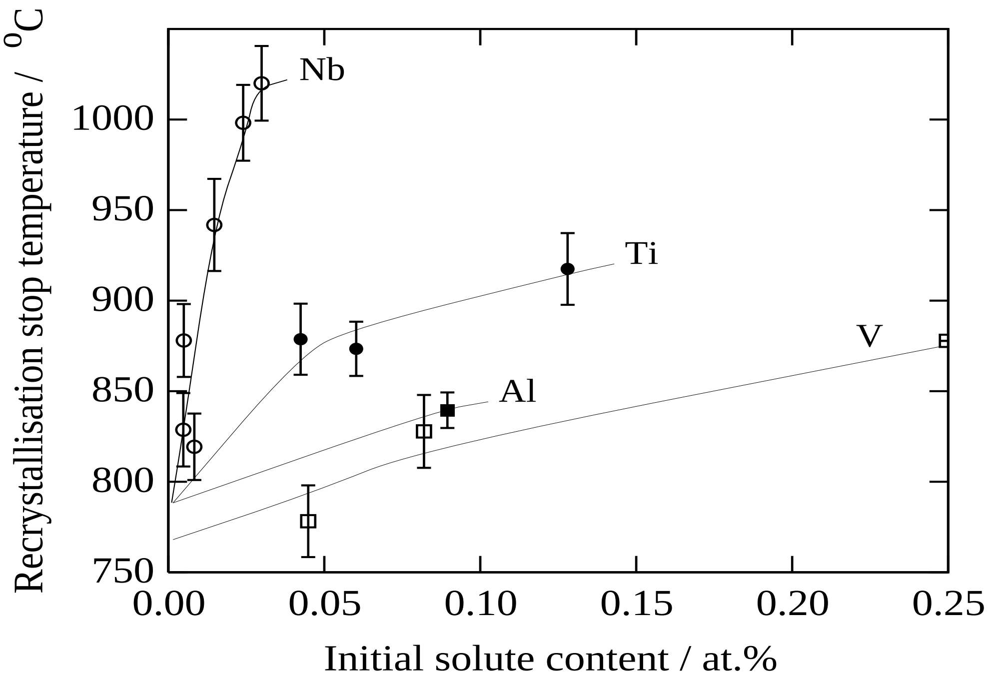

Fig. 14: The effects of microalloying elements on the recrystallisation temperature of austenite in a low carbon steel [20].

By suppressing recrystallisation, they allow a higher fraction of the strain to be retained in austenite. This increases the ferrite nucleation rate during subsequent cooling and a finer ferrite grain size is obtained. Nb is more effective than V in refining the grains. Abe *et al.* [16] and Irvine *et al.* [15] have observed a finer ferrite grain size in niobium steel than in comparable vanadium steel. A larger concentration of vanadium is required to achieve the same effect as niobium [15]. Interphase precipitation also causes grain refinement by hindering the ferrite grain growth [22].

At the same grain size microalloyed steels have higher strength than the plain C–Mn steels [15], and this has been attributed to the presence of fine precipitates of carbides and nitrides of the microalloying elements. In this respect V is more effective than Nb particularly at higher nitrogen contents [23].

Both Nb and V also increase the hardenability and reduce the ferrite transformation temperature [16, 22].

These characteristics are predicted using the neural network model as shown in Fig. 15. A 0.02 wt.% increase in Nb, in the region in which the error bars are small, increases the yield strength by about 40 MPa and the tensile strength by 25 MPa whilst the same amount of V

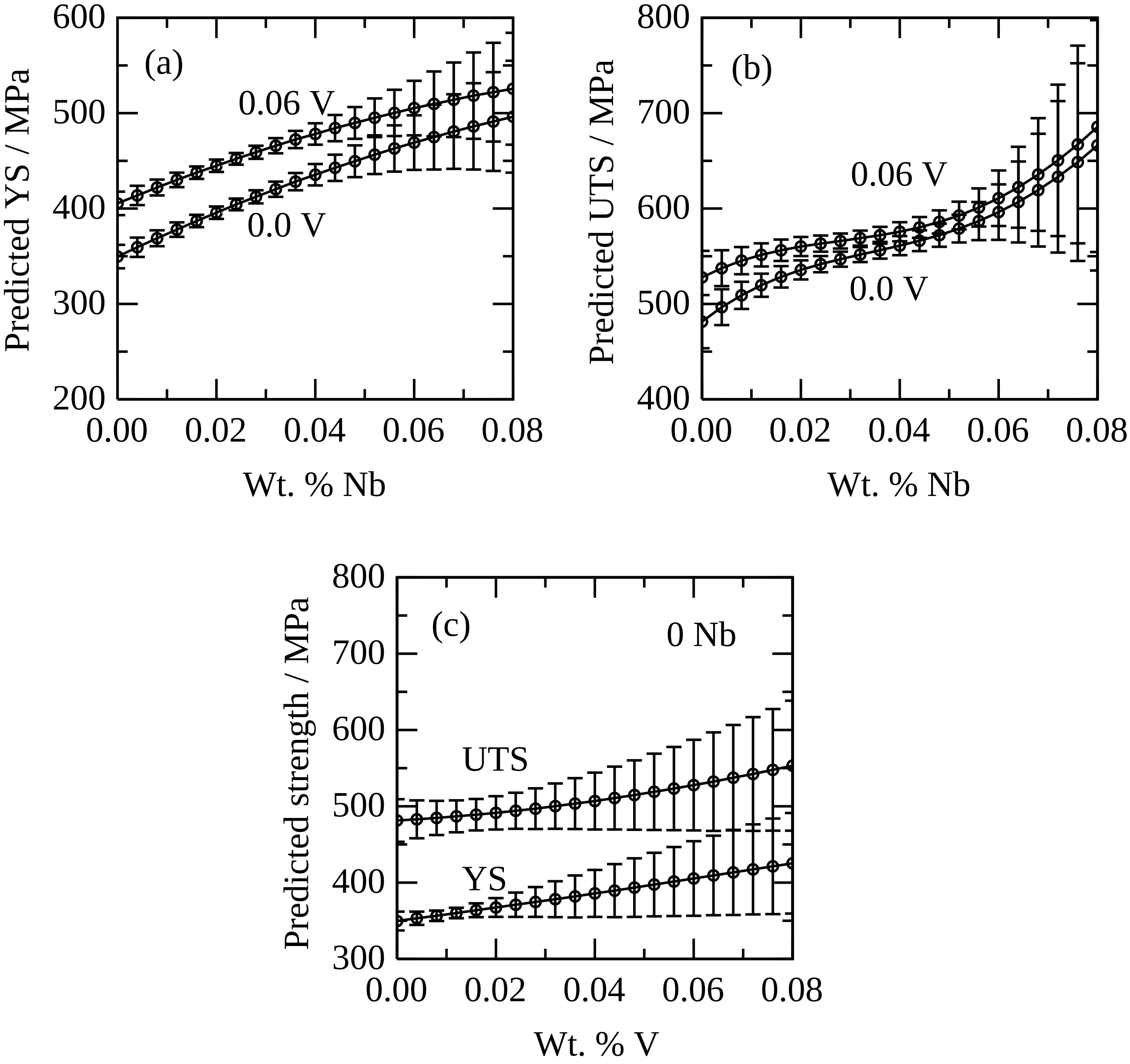

Fig. 15: The effect of niobium and vanadium on the yield and tensile properties. Normally V is not added alone but is combined with Nb. The calculations are presented here for illustration only.

increases both the YS and the UTS by only 15 MPa. The experimental results reported in literature more or less confirm these model predictions [12, 15–17, 24].

Fig. 15 also highlights the fact that a combined addition of V and Nb enhances the strengthening effects, consistent with the experimental results reported by Irvine *et al.* [15]. They found that an addition of 0.06 wt.% of V to a Nb microalloyed steel raises the yield strength by about 40 MPa and the UTS by a smaller increment of 15 MPa.

Rolling Parameters

Fig. 16 shows the effect of 1 st pass reduction on the yield and ultimate tensile strengths; both increase as the pass reduction is increased with the yield strength showing a greater variation. Fig. 16 is an extrapolation over the normal rolling practice. Usually the first pass reduction is less than 10% and in some cases it may be preceded by a few unrecorded cogging passes. It should also be noted that the effect shown in Fig. 16 is not of the pass reduction alone. Other factors need to be taken into account. The percentage reduction in all other passes were kept constant so that for a given slab thickness, a higher 1 st pass reduction meant a lower gauge at all other stages of rolling and hence a thinner final plate gauge. It follows that with increasing 1 st pass reduction all other subsequent passes are executed at lower temperatures due to the thinner gauge.

The effect of increasing (1) the initial slab thickness to 400 mm and (2) the 9 th pass delay time (delay before 9th pass) to 500 s from 24 s is also included in Fig. 16. A slab thickness of 400 mm is used here as an example only.

The effect of increasing the slab thickness to 400 mm without changing the pass reductions is to lower the strength, which is reasonable. For reasons already discussed, the introduction of a delay period of 500 seconds before the 9 th pass raises the strength.

In the above discussion, the percent reduction of only one pass was systematically varied. This has the effect of changing the final plate thickness. We now present some calculations where the reductions for two or more passes were simultaneously varied in such a way that the final plate thickness is not altered. The slab thickness, the delay times and the pass times were not changed and the reductions for the other passes are the same as in Table 1. Fig. 17a shows the lack of variation in strength for a case where the 1 st pass reduction was increased together with a corresponding decrease in the 19 th (the last) pass reduction which left the final plate thickness unaltered at 8.1 mm for a 200 mm starting slab. This is because a small first pass reduction leads to a higher temperature for all subsequent passes including the last pass with a high reduction since none of the delay times is altered, so that the strength does not increase. When the 1st pass reduction is large, the later passes occur at a lower temperature. It is suggested that the resultant of these two effects is that the strength does not vary.

Similar results were obtained when the schedule given in Table 1 was modified. The 15 th and the 16 th pass strain were set to zero but the 4 th and the 5th pass strains were increased equally so that the final plate thickness remained 13.8 mm. The effect of this change in schedule on the variation of YS and UTS with C is illustrated in Fig. 17b. A comparison with Fig. 10a makes it obvious that the change in schedule has not made much of a difference to the properties.

We have already seen that the introduction of a delay time can have an effect on the final mechanical properties if it leads to grain refinement. Naturally, this can only be significant at the late stages of rolling and this is reflected in the results presented in Fig. 18.

Optimisation of YS/UTS ratio

The YS/UTS ratio is an important design criterion for many fail–safe applications where a low value is desired. Examples include earthquake resistant steels and cases where a good fatigue resistance is required [25].

The present model was used to explore the possibility of designing such a steel. The effect of variations in the carbon and manganese concentrations on the ratio are summarised in Fig. 19.

The ratio decreased with increasing C concentration. As argued earlier, this is because the pearlite content increases with C which affects UTS more than the YS. However, a very high carbon is not acceptable because of its adverse effect on weldability and toughness. Low C will not give adequate strength. Mn raises the ratio mainly due to its influence on ferrite grain size which raises the YS more than the UTS. Other factors which affect the YS/UTS ratio are the delay period and the plate thickness. These have already been discussed.

Other Published Data

Irvine *et al.* [15] have systematically studied the effect of chemical composition on the final properties of steel in the as–rolled and normalised conditions (Table 2). The present model

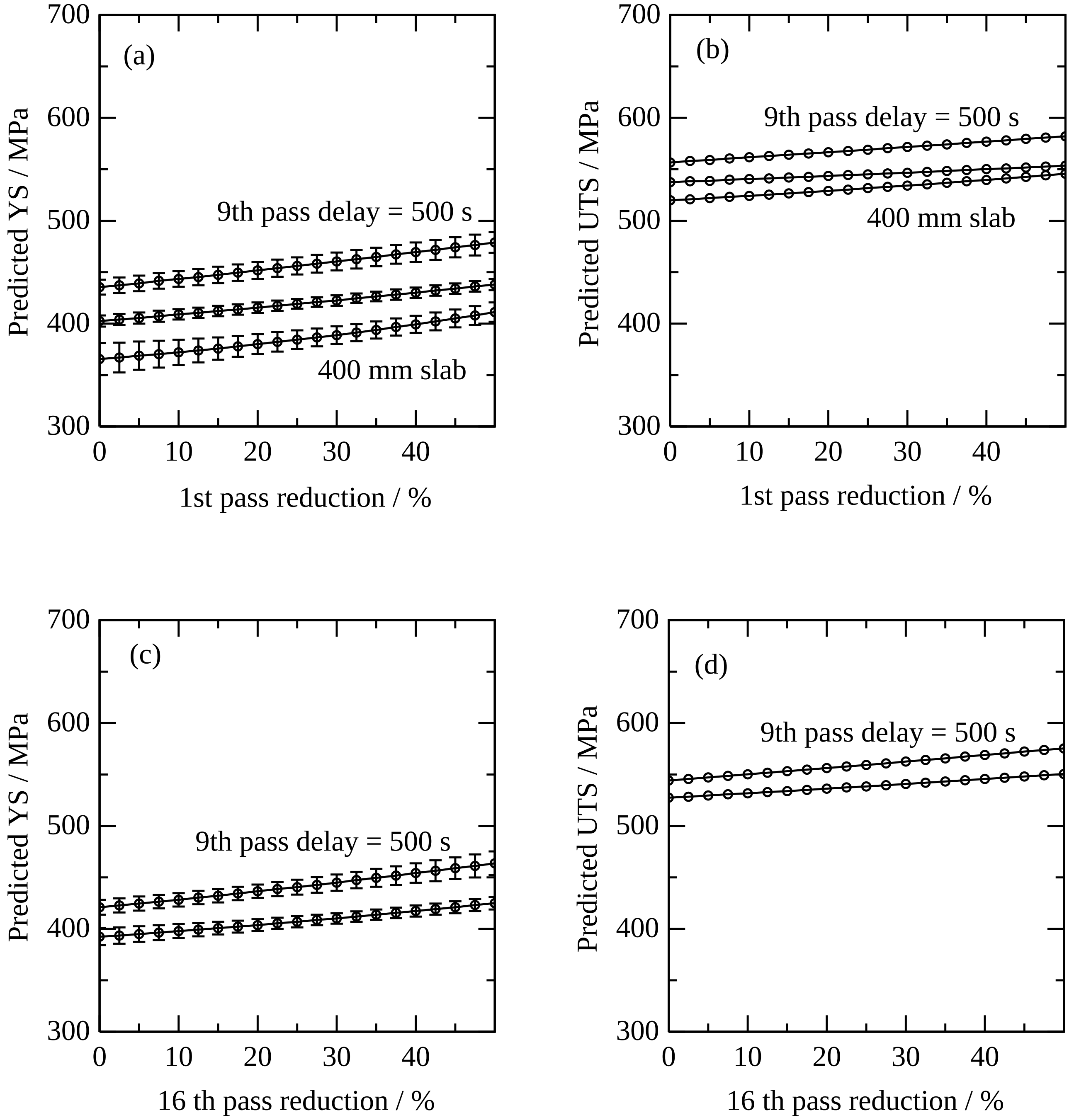

Fig. 16: (a,b) The effect of 1 st pass reduction on the yield and ultimate tensile strengths. (c,d) The corresponding effects as a function of the 16 th pass reduction.

was tested against their results. In their experiments the samples were reheated to 1200 °C and the finish rolling temperature was about 900 °C. They have not reported the details of rolling schedule employed and for the present calculation it has been assumed that they are similar to the standard conditions used here. It is clear that the model predicts the data rather well (Fig. 20 and Table 3).

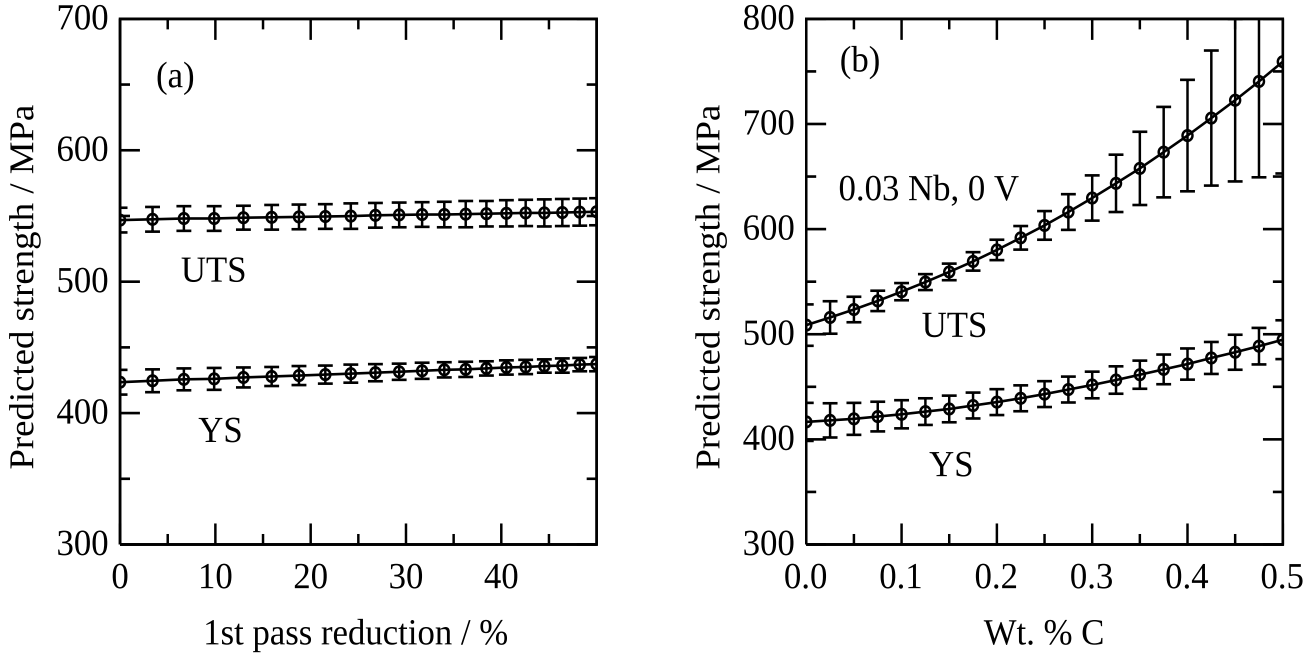

Fig. 17: (a) Effect of a simultaneous variation of first and last pass strain keeping the final plate thickness constant. (b) The effect of a modification of the schedule given in Table 1 in such a way that the final plate thickness was the same.

CONCLUSIONS

A neural network model capable of predicting the yield and tensile strengths of steel plates as a function of composition and rolling parameters has been trained and tested. The model has been shown to be consistent with established metallurgical trends and can, for example, be used to study the effect of each variable in isolation. There are interesting results on the yield to tensile strength ratio whose value can be altered systematically by controlling the carbon and manganese concentrations.

ACKNOWLEDGMENTS

The authors are grateful to British Steel plc for financial support and to Dr. K. Melton, Research Director Swinden Technology Center for permission to publish this paper. We thank Professor A. H. Windle for the provision of laboratory facilities at the University of Cambridge. We also thank Mr. John Street for his help in setting up the database required for the analysis. SBS thanks Cambridge Commonwealth trust for a scholarship.

REFERENCES

1) T. Gladman, *The Physical Metallurgy of Microalloyed Steels,* The Institute of Materials, London, 1997.

2) D. J. C. MacKay, *Mathematical Modelling of Weld Phenomena 3,* (eds. H. Cerjack and H. K. D. H. Bhadeshia), Institute of Materials, London 1997 359.

3) D. J. C. MacKay, *Neural Computation,* **4** 1992 415.

4) D. J. C. MacKay, *Neural Computation,* **4** 1992 448.

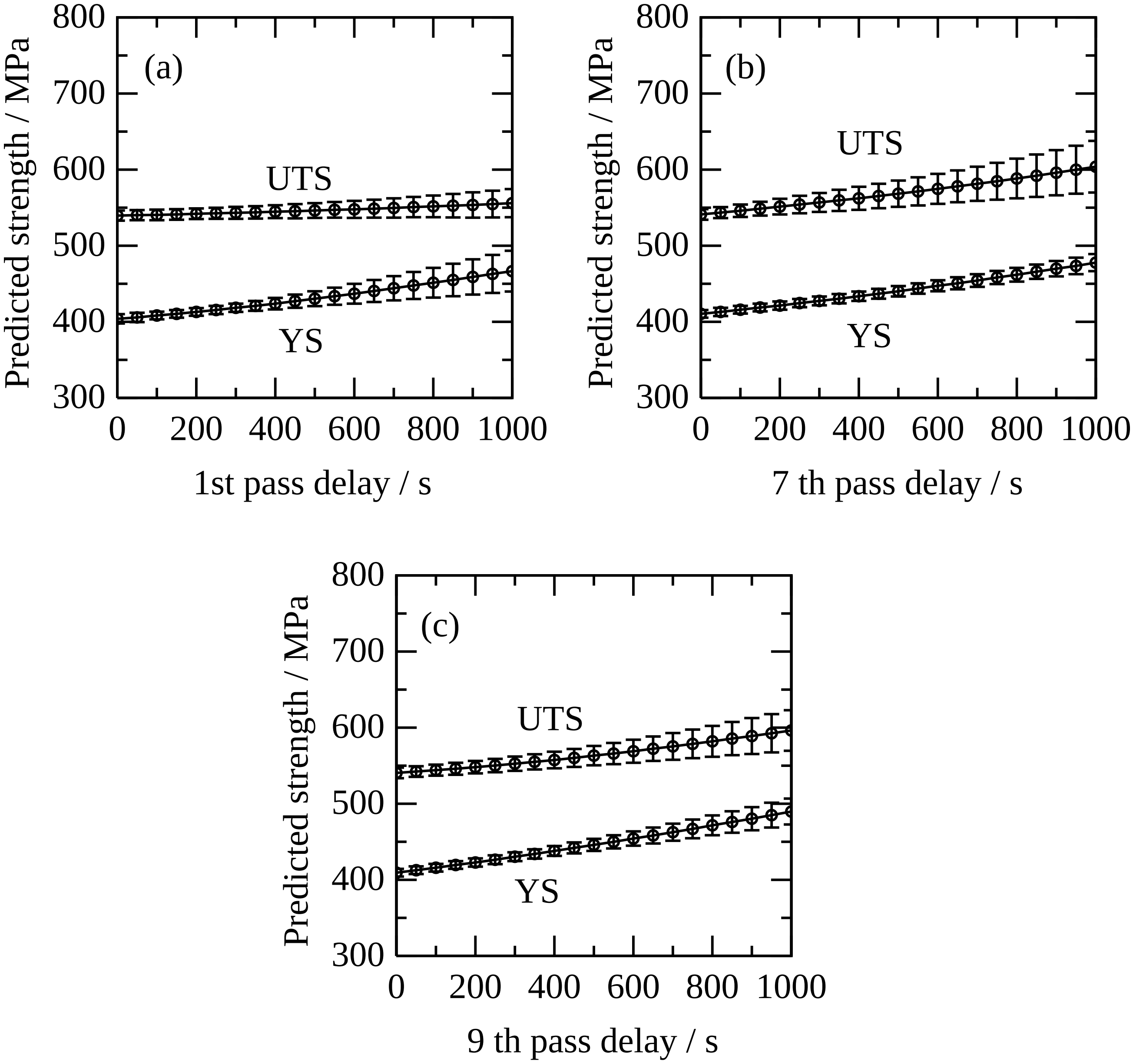

Fig. 18: Effect of delay time on yield and tensile strengths.

5) D. J. C. MacKay, *ASHRAE (American Society of Heating, Refrigerating and Air–conditioning Engineers) Transactions,* **100, pt. 2** 1994 1053.

6) D. J. C. MacKay, *Network: Computation in Neural Systems,* **6** 1995

7) H. K. D. H. Bhadeshia, D. J. C. MacKay and L.–E. Svensson, *Materials Science and Technology,* **11** 1995 1046.

8) R. M. Neal, *Bayesian Learning for Neural Networks* Springer, 1996

9) R. W. K. Honeycombe and H. K. D. H. Bhadeshia, *Steels Microstructure and Preoperties* Edward Arnold, 1995.

10) F. B. Pickering, *Physical Metallurgy and the Design of Steels* Allied Science Publishers, London, 1978.

11) P. D. Hodgson and R. K. Gibbs, *ISIJ International* **32** 1992 1329.

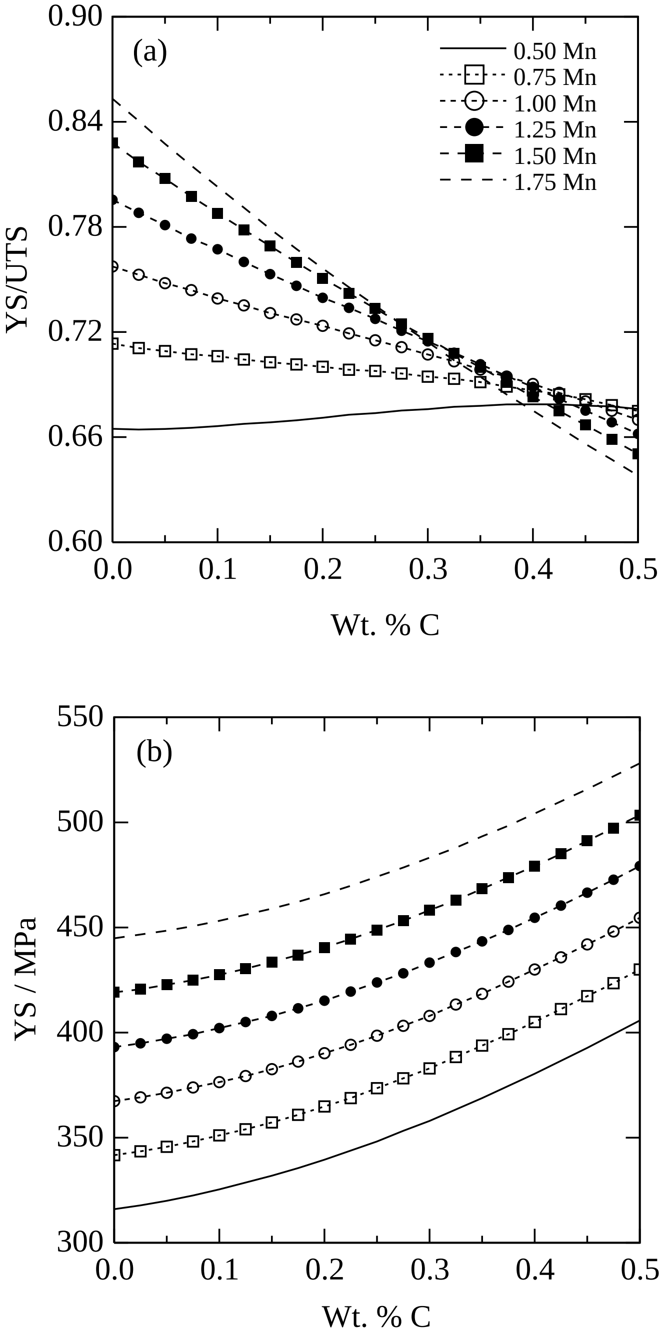

Fig. 19: The effect of carbon and manganese on YS/UTS ratio and the yield strength.

12) M. Shimizu, M. Hiromatsu, S. Takashima, H. Kaji and M. Kano, *HSLA Steels: Metallurgy and Application,* (eds. J. M. Gray, T. Ko, Z. Shouhua, W. Baorong and X. Xishan), ASM Int. OH, 1986 591.

13) W. C. Leslie, *The Physical Metallurgy of Steels* McGraw–Hill Book Company, 1981.

14) W. B. Morrison, *Trans. ASM* **59** 1966 824

15) K. J. Irvine, F. B. Pickering and T. Gladman, *JISI* **210** 1967 161.

16) T. Abe, K. Tsukada and I. Kozasu, *HSLA Steels: Metallurgy and Application,* (eds. J. M. Gray, T. Ko, Z. Shouhua, W. Baorong and X. Xishan), ASM Int. OH, 1986 103.

17) M. Cohen and S. S. Hansen, *HSLA Steels: Metallurgy and Application,* (eds. J. M.

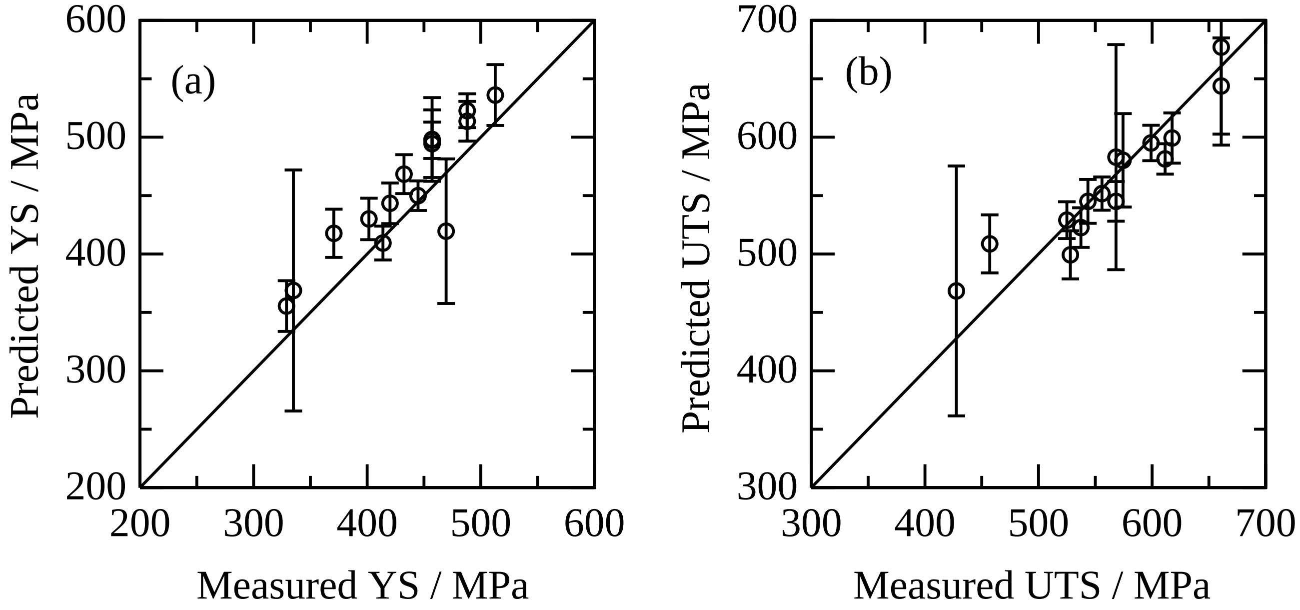

Fig. 20: Comparison of the predicted YS and UTS with experiments reported in literature [15]. Please note that these experiments were not included in the training database.

Steel	C	Mn	Si	Al	N	Nb	V
1	0.10	0.60	0.41	–	–	0.08	–
2	0.10	0.50	0.1	–	0.013	–	0.095
3	0.15	1.39	0.22	0.039	0.015	–	–
4	0.05	1.30	0.09	–	0.0072	0.037	–
5	0.044	1.42	0.24	–	0.0088	0.048	0.058
6	0.099	1.35	0.26	–	0.0076	0.044	–
7	0.104	1.43	0.27	–	0.0080	0.047	0.075
8	0.151	1.48	0.27	–	0.0080	0.047	–
9	0.149	1.49	0.32	–	0.0088	0.049	0.070
10	0.046	1.40	0.27	–	0.0138	0.037	–
11	0.040	1.31	0.26	–	0.0172	0.043	0.072
12	0.083	1.32	0.16	–	0.016	0.03	–
13	0.085	1.36	0.13	–	0.0154	0.04	0.070
14	0.148	1.43	0.23	–	0.0142	0.04	–
15	0.144	1.48	0.22	–	0.0144	0.05	0.08

Table 2 : Chemical compositon of the steels studied by Irvine et al. [15]. The concentrations are in wt%.

Gray, T. Ko, Z. Shouhua, W. Baorong and X. Xishan), ASM Int. OH, 1986 61.

Steel	Measured YS / MPa	Predicted YS / MP	Measured UTS / MPa	Predicted UTS / MPa
1	469.5	419.5	568.2	582.9
2	335.0	368.7	427.7	468.4
3	328.9	355.4	528.0	499.2
4	370.7	417.7	457.0	508.7
5	457.2	497.3	568.2	545.0
6	420.0	443.4	555.8	551.7
7	488.0	513.6	617.6	599.2
8	432.4	468.4	599.1	595.0
9	488.0	522.7	660.8	643.8
10	401.5	430.0	524.9	528.9
11	457.1	494.4	543.5	545.0
12	413.9	409.4	537.3	522.6
13	457.1	498.0	574.4	580.2
14	444.8	449.5	611.4	581.4
15	512.8	536.1	660.8	677.1

Table 3: Comparison of the predicted yield and tensile strengths with those reported in literarure [15]

18) T. Gladman *et al.* , *Microalloying 75* Union Carbide Corporation, 1975.

19) R. K. Amin and F. B. Pickering, *Thermomechanical Processing of Microalloyed Austenite* (eds. A. J. DeArdo, G. A. Ratz and P. J. Wray) TMS–AIME, Warrendale, PA 1981 1.

20) L. J. Cuddy, *Thermomechanical Processing of Microalloyed Austenite* (eds. A. J. DeArdo, G. A. Ratz and P. J. Wray) TMS–AIME, Warrendale, PA 1981 129.

21) F. Boratto, R. Barbosa, S. Yue and J. J. Jonas, *Proc. Int. Conf. on Physical Metallurgy of Thermomechanical Processing of Steel and other Metals (Thermec-88)* (ed. I. Tamura), ISIJ, Tokyo, 1988 383.

22) R. K. Amin and F. B. Pickering, *Thermomechanical Processing of Microalloyed Austenite* (eds. A. J. DeArdo, G. A. Ratz and P. J. Wray) TMS–AIME, Warrendale, PA 1981 377.

23) K. J. Irvine and F. B. Pickering, *JISI* **201** 1963 944.

24) J. Lessells, *HSLA Steels: Metallurgy and Application,* (eds. J. M. Gray, T. Ko, Z. Shouhua, W. Baorong and X. Xishan), ASM Int. OH, 1986 613.

25) H. K. D. H. Bhadeshia, *Bainite in Steels* The Institute of Materials, London, 1992.

APPENDIX 1

Table 4: The variables, with concentrations stated in wt%. S(J)=screw setting, in mm, for Jth pass; D(J)= delay time, in seconds, before J'th pass and T(J)=J'th pass time in seconds.

Variable	Range	Mean	Standard deviation
Reheat temp., $^{\circ}C$	993–1373	1212	22.98
Slab gauge, mm	161–600	245.1	36.25
Slab length, mm	915–4080	2828	700.6
C	0.076–0.25	0.14	0.036
Mn	0.7–1.54	1.29	0.24
Si	0.14–0.46	0.32	0.07
S	0.001–0.019	0.006	0.004
P	0.008–0.027	0.015	0.003
Ni	0.014–0.56	0.038	0.045
Cr	0.01–0.53	0.028	0.047
Mo	0.001–0.017	0.003	0.0014
Cu	0.004–0.296	0.032	0.049
Al	0–0.058	0.036	0.008
N	0–0.011	0.005	0.002
Nb	0–0.043	0.024	0.014
V	0.001–0.063	0.009	0.016
Ti	0–0.033	0.0019	0.0017
S(1)	91.0–354.9	190.3	40.67
D(1)	47.0–736.0	144.3	58.05
T(1)	1.0–3.0	1.5	0.51
S(2)	80.1–343.1	175.4	39.75
D(2)	5.0–39.0	7.3	1.77
T(2)	1.0–5.0	2.2	0.92
S(3)	66.1–328.1	161.1	38.44
D(3)	5.0–105.0	14.4	10.34
T(3)	1.0–25.0	1.5	0.75
S(4)	64.5–311.2	150.0	37.02
D(4)	4.0–198.0	12.16	6.58
T(4)	1.0–6.0	2.4	1.19

Table 4 contd...

Variable	Range	Mean	Standard deviation
S(5)	46.0–288.6	130.6	36.43
D(5)	5.0–1163.0	48.4	160.24
T(5)	1.0–9.0	2.0	0.80
S(6)	34.4–268.0	119.1	36.66
D(6)	3.0–263.0	10.0	8.24
T(6)	1.0–9.0	2.6	0.87
S(7)	26.8–249.1	103.9	35.99
D(7)	5.0–986.0	72.1	181.24
T(7)	1.0–5.0	2.5	0.91
S(8)	21.3–232.1	92.2	35.66
D(8)	4.0–43.0	8.0	3.66
T(8)	1.0–7.0	3.1	1.03
S(9)	15.7–216.9	79.3	33.20
D(9)	0.0–894.0	102.1	218.45
T(9)	0.0–48.0	3.4	1.67
S(10)	12.9–203.5	69.3	31.32
D(10)	0.0–170.0	6.7	5.28
T(10)	0.0–19.0	4.0	1.71
S(11)	11.1–192.0	60.3	28.94
D(11)	0.0–910.0	41.8	128.62
T(11)	0.0–16.0	4.4	1.81
S(12)	8.8–182.4	53.5	26.97
D(12)	0.0–660.0	7.0	17.71
T(12)	0.0–20.0	4.9	2.19
S(13)	8.0–174.0	47.9	24.65
D(13)	0.0–735.0	24.0	84.84
T(13)	0.0–15.0	5.0	2.41
S(14)	5.8–167.2	43.7	22.85
D(14)	0.0–163.0	6.3	6.03
T(14)	0.0–28.0	5.3	2.98

Table 4 *contd...*

Variable	Range	Mean	Standard deviation
S(15)	7.0–161.6	40.5	20.75
D(15)	0.0–790.0	20.6	84.70
T(15)	0.0–15.0	4.7	3.04
S(16)	5.3–157.1	38.0	19.33
D(16)	0.0–163.0	5.9	8.02
T(16)	0.0–26.0	5.0	3.62
S(17)	7.7–153.8	36.3	17.91
D(17)	0.0–497.0	6.5	19.64
T(17)	0.0–17.0	3.9	3.42
S(18)	7.9–151.3	34.9	16.98
D(18)	0.0–111.0	4.9	7.43
T(18)	0.0–21.0	4.2	4.12
S(19)	7.9–150.2	33.9	16.17
D(19)	0.0–193.0	4.3	8.14
T(19)	0.0–17.0	3.1	3.72
S(20)	7.9–150.2	33.1	15.57
D(20)	0.0–86.0	4.1	7.74
T(20)	0.0–27.0	3.1	4.02
S(21)	7.9–150.2	32.5	15.16
D(21)	0.0–183.0	4.2	14.35
T(21)	0.0–15.0	2.4	3.66
S(22)	7.6–150.2	32.1	14.87
D(22)	0.0–142.0	3.4	8.78
T(22)	0.0–19.0	2.4	3.78
S(23)	7.6–150.2	31.8	14.72
D(23)	0.0–172.0	4.4	16.45
T(23)	0.0–16.0	1.8	3.40
S(24)	7.9–150.2	31.5	14.60
D(24)	0.0–121.0	2.2	6.60
T(24)	0.0–14.0	1.7	3.35

Table 4 *contd...*

Variable	Range	Mean	Standard deviation
S(25)	7.9–150.2	31.4	14.45
D(25)	0.0–295.0	2.9	15.97
T(25)	0.0–13.0	1.2	2.81
S(26)	7.9–50.2	31.3	14.38
D(26)	0.0–107.0	1.6	6.19
T(26)	0.0–15.0	1.2	3.12
S(27)	7.9–150.2	31.2	14.30
D(27)	0.0–112.0	1.1	5.60
T(27)	0.0–13.0	0.7	2.21
S(28)	6.7–150.2	31.2	14.29
D(28)	0.0–136.0	1.3	7.50
T(28)	0.0–15.0	0.5	2.05
S(29)	7.9–150.2	31.2	14.25
D(29)	0.0–40.0	0.4	2.02
T(29)	0.0–12.0	0.2	1.05
S(30)	7.2–150.2	31.1	14.25
D(30)	0.0–64.0	0.5	4.57
T(30)	0.0–10.0	0.1	0.92
Condition	0 or 1	—	—
YS, MPa	232.0–594.0	398.5	66.64
UTS, MPa	389–692	537.5	44.07